REPORT DOCUMENTATION PAGE

Form Approved OMB NO. 0704-0188

1. REPORT DATE (DD-MM-YYYY)	2. REPORT TYPE	3. DATES COVERED (From - To)
05-02-2020	Final Report	1-Jul-2016 - 30-Nov-2019

4. TITLE AND SUBTITLE
Final Report: Synthesis and Processing of Materials: Directional Recrystallization Processing

5a. CONTRACT NUMBER
W911NF-16-1-0367

5b. GRANT NUMBER

5c. PROGRAM ELEMENT NUMBER
611102

6. AUTHORS

5d. PROJECT NUMBER

5e. TASK NUMBER

5f. WORK UNIT NUMBER

7. PERFORMING ORGANIZATION NAMES AND ADDRESSES
Dartmouth College
11 Rope Ferry Rd.

Hanover, NH 03755 -1404

8. PERFORMING ORGANIZATION REPORT NUMBER

9. SPONSORING/MONITORING AGENCY NAME(S) AND ADDRESS (ES)
U.S. Army Research Office
P.O. Box 12211
Research Triangle Park, NC 27709-2211

10. SPONSOR/MONITOR'S ACRONYM(S)
ARO

11. SPONSOR/MONITOR'S REPORT NUMBER(S)
69027-MS.3

12. DISTRIBUTION AVAILIBILITY STATEMENT
Approved for public release; distribution is unlimited.

13. SUPPLEMENTARY NOTES
The views, opinions and/or findings contained in this report are those of the author(s) and should not contrued as an official Department of the Army position, policy or decision, unless so designated by other documentation.

14. ABSTRACT

15. SUBJECT TERMS

16. SECURITY CLASSIFICATION OF:			17. LIMITATION OF ABSTRACT	15. NUMBER OF PAGES	19a. NAME OF RESPONSIBLE PERSON
a. REPORT	b. ABSTRACT	c. THIS PAGE			Ian Baker
UU	UU	UU	UU		19b. TELEPHONE NUMBER 603-646-2184

RPPR Final Report
as of 06-Feb-2020

Agency Code:

Proposal Number: 69027MS **Agreement Number: W911NF-16-1-0367**
INVESTIGATOR(S):

Name: Ian Baker Ph.D.
Email: Ian.Baker@Dartmouth.edu
Phone Number: 6036462184
Principal: Y

Organization: **Dartmouth College**
Address: 11 Rope Ferry Rd., Hanover, NH 037551404
Country: USA
DUNS Number: 041027822 EIN: 020222111
Report Date: 29-Feb-2020 Date Received: 05-Feb-2020
Final Report for Period Beginning 01-Jul-2016 and Ending 30-Nov-2019
Title: Synthesis and Processing of Materials: Directional Recrystallization Processing
Begin Performance Period: 01-Jul-2016 **End Performance Period:** 30-Nov-2019
Report Term: 0-Other
Submitted By: Ian Baker Email: Ian.Baker@Dartmouth.edu
Phone: (603) 646-2184
Distribution Statement: 1-Approved for public release; distribution is unlimited.

STEM Degrees: **STEM Participants:**

Major Goals: The goal of this project was to explore how microstructural parameters (solutes, particle size/spacing, texture) interact with the processing conditions (temperature, rate of hot zone movement,) to influence microstructural evolution during directional recrystallization (DR), and thereby gain fundamental understanding of the DR process.

Accomplishments: PDF document uploaded in "Upload" section

Training Opportunities: Nothing to Report

Results Dissemination: [1] “The Effects of Solute and Particles on the Microstructure Changes during Directional Annealing in a Ni-Al System”, C. Yang and I. Baker, TMS Annual meeting, San Antonio, Texas, March 10-14, 2019.

[2] “Directional Recrystallization Processing”, I. Baker, Invited talk to be presented at the Symposium on “Purveyors of Processing Science and ICME: A SMD Symposium to Honor the Many Contributions of Taylan Altan, Wei Tsu Wu, Soo-Ik Oh, and Lee Semiatin”, 2020 TMS Annual Meeting, San Diego, CA, February 23-27th, 2020.

Honors and Awards: Nothing to Report

Protocol Activity Status:

Technology Transfer: Nothing to Report

PARTICIPANTS:

Participant Type: Graduate Student (research assistant)
Participant: Chao Yang
Person Months Worked: 11.00 **Funding Support:**
Project Contribution:
International Collaboration:
International Travel:
National Academy Member: N
Other Collaborators:

RPPR Final Report
as of 06-Feb-2020

ARTICLES:

Publication Type: Journal Article Peer Reviewed: Y **Publication Status:** 1-Published
Journal: Philosophical Magazine
Publication Identifier Type: DOI Publication Identifier: 10.1080/14786435.2019.1576936
Volume: 99 Issue: 9 First Page #: 1057
Date Submitted: 4/3/19 12:00AM Date Published: 2/1/19 5:00AM
Publication Location: 5 Howick PlWestminster, London SW1P 1BH, UK
Article Title: Elevated temperature directional recrystallization of high-purity nickel
Authors: Chao Yang, Ian Baker
Keywords: recrystallization, grain grow, nickel, soulute effect
Abstract: Electron backscattered di?raction has been used to characterise the three di?erent kinds of boundaries that occur in grains that are generated by secondary recrystallization during directional annealing of high-purity nickel. Boundaries between columnar grains (CC boundaries) can be twin boundaries, low-angle boundaries or high-angle grain boundaries. The frequency of low-angle CC boundaries dropped from 25% to 0% while the frequency of the high-angle CC boundaries increased from 19% to 67% when the annealing temperature was increased from 1000°C to 1200°C. The misorientation angles of boundaries between columnar grains and small equiaxed grains ahead of them (CE boundaries) was random at 1200°C but had a 40° rotation relationship about ?111? at 1000°C. It was found out that the character of the CC boundaries is determined by relative mobility of the CE boundaries, which is determined by the processing temperature rather than the energy of the CC boundaries themselves. The character of
Distribution Statement: 3-Distribution authorized to U.S. Government Agencies and their contractors
Acknowledged Federal Support: **Y**

Publication Type: Journal Article Peer Reviewed: Y **Publication Status:** 1-Published
Journal: Philosophical Magazine Letters
Publication Identifier Type: ISSN Publication Identifier: 0950-0839
Volume: 99 Issue: 5 First Page #: 167
Date Submitted: 8/26/19 12:00AM Date Published: 7/22/19 4:00AM
Publication Location: United Kingdom
Article Title: Breakdown of growth front at elevated drawing velocity during directional recrystallization
Authors: Chao Yang, Ian Baker
Keywords: Directional recrystallization; grain growth; Nickel; EBSD; growth competition
Abstract: Cold-rolled, high-purity Ni was directionally annealed at a variety of drawing velocities to understand how columnar grains behave when the drawing velocity was increased during processing. It is shown that the upper limit of drawing velocity for columnar grain propagation is higher than that for columnar grain nucleation in accordance with a prediction of previous modelling (Badmos et al., Acta Mater., 50 (2002) 8). When the drawing velocity was increased during columnar grain propagation, there are always some columnar grains or some part of a columnar grain that stopped growing, which leads to a breakdown of the growth front. Electron backscatter diffraction showed that the breakdown was either because the growing grains were not the {124} < 211 >orientation with a 40?/ <111> misorientation with respect to the cube texture into which the grains were growing, or parts of the columnar grain were locally pinned by low CSL or low-angle misorientation boundaries ahead of them. In general
Distribution Statement: 3-Distribution authorized to U.S. Government Agencies and their contractors
Acknowledged Federal Support: **Y**

RPPR Final Report
as of 06-Feb-2020

Objectives

The primary objectives include:

1. Use a low aluminum concentration nickel alloy to understand the effect of solute on the microstructural evolution during DR.
2. Use a high aluminum concentration nickel alloy with different heat treatment times to investigate the effects of particle size and distribution on the microstructural evolution during DR.
3. Determine how the processing conditions (temperature, rate of hot zone movement) affect the microstructural evolution during DR for different solute concentrations and particles.
4. Develop a model to understand the effects of solute and particles on DR.

Approach

Our approach includes:

- casting Ni-Al alloys with two different solute concentrations
- homogenization anneals of the cast alloys
- heat treat to precipitate particles with different sizes and distributions
- using transmission electron microscope (TEM) and scanning electron microscope (SEM) analysis to characterize the particle size and dispersion
- cold-rolling alloys and pure nickel to a 99% rolling reduction

- determining the texture and generating orientation images using electron backscatter patterns (EBSPs) of the rolled alloys and pure nickel
- directionally annealing the cold-rolled alloys and pure nickel at different temperatures and hot zone velocities
- analyzing the resulting microstructures using EBSPs and a TEM.

Details are given below.

1. *Alloy Preparation:* We had two Ni-Al alloys cast commercially with two Al concentrations. One has a solute concentration of 3 at. % Al, which is below the solubility limit of Al in Ni at room temperature. This alloy is used to examine the effects of a solute on DR. A second alloy has a solute concentration of 12 at. % Al. Based on the phase diagram, this alloy should contain 30 volume percent Ni_3Al precipitates at room temperature: the precipitates will completely dissolve at processing temperatures >900°C. This alloy is being used to exam the effect of particles on DR. After casting, both alloys were homogenized by annealing at 1000°C for 24 h. After this solution treatment, the Ni-12 at. % Al was annealed at 700°C for either 30 minutes or 48 hours to provide Ni_3Al particles with different particle sizes and distributions.
2. *Determination of Dispersion Parameters:* The particle size and distribution were determined using a FEI Technai F2 Field Emission Gun (FEG) TEM after twin-jet polishing and a Technai XL30 FEG SEM after electro-polishing. Image J was used for particle size analysis.
3. *Processing, and Parameter Determination:* The alloys and pure nickel were cold-rolled to

99% rolling reduction to ~1 mm thick and then annealed at temperatures from 500-1100°C to determine the primary and secondary recrystallization temperature. Our FEI Scios SEM enables very rapid determination of grain orientations and grain boundary misorientations both before and after recrystallization using electron backscattered diffraction (EBSD).

4. *Directional Annealing:* The cold rolled alloys and pure nickel were directionally annealed in air using a variety of hot zone temperatures (determined by the aforementioned isothermal annealing) and hot zone velocities of 2-200 mm/h using a modified Tsukuba Asgal Model F2SS35W optical-image single crystal-growing furnace. Spring-loaded, water-cooled plates were used to produce a temperature gradient of 1000°C/cm ahead of the hot zone.

5. *Directionally Annealed Microstructures:* Optical microscopy and EBSPs were used to analyze the microstructure and determine the grain orientations and grain boundary misorientations of the DR samples. The analyses focuses not only on the DR region, but also the region ahead of the DR region.

Tasks Completed

The following tasks were completed:

1. A systematic investigation of how a solute interacts with processing conditions (temperature, drawing velocity) to influence microstructural evolution during directional recrystallization were performed by comparing Ni-3Al and high-purity Ni DRed at 1000°C, 1100°C and 1200°C at various drawing velocities. How solute induced a character change in the grain boundaries, texture and grain morphology was systematically studied.

2. A systematic investigation of how soluble particles interact with processing conditions (temperature, drawing velocity) to influence microstructural evolution during directional recrystallization were performed by comparing Ni-12Al and Ni-3Al at 1000°C, 1100°C and 1200°C at various drawing velocities. How soluble particles induced a change in grain boundary character, textures and grain morphology was systematically studied. The effect of how texture affects DR was also studied.

3. How columnar grains behave when the drawing velocity was increased during processing was studied using high-purity Ni, which was used to firm a prediction of previous front-tracking modeling (Badmos et al., Acta Materialia, **50** (2002) 8).

Results

TEM characterization of particles before and after directional recrystallization.

Figure 1 (a) shows a bright field image of a sample isothermally annealed at 700°C for 48 h after homogenization at 1000°C for an hour. The corresponding diffraction pattern taken a [001] zone is shown in Figure 1 (b). Figure 1 (c) shows a dark field image of the sample isothermally annealed at 700°C for 30 min after homogenization at 1000°C for an hour with its corresponding diffraction pattern taken at [001] in Figure 1 (d). The presence of superlattice reflections indicates that the particles have a $L1_2$ structure, which is Ni_3Al in this material. The superlattice reflections in the 48h annealed sample are sharp while the spots are weak in the 30 min annealed sample. 100 precipitates were analyzed in each sample. The 48h annealed samples and the 30 min annealed samples had mean particle sizes of 358+68 nm and 41+9 nm, respectively, which are called large-particle samples and small-particle samples hereforth.

Figure 2 (a) shows a bright field image of a small particle sample DRed at 1200°C, 10 mm/h with its corresponding diffraction pattern taken near the [001] zone (Figure 2 (b).) Figure 2 (c) shows bright field image of a large-particle sample DRed at 1200°C, 10 mm/h with its corresponding diffraction pattern taken at the [001] zone (Figure 2 (d).) The disks were taken from a region in which obvious grain growth had occurred. It is shown that there are no particles after grain growth in either small-particle samples or large-particle samples. Note that there are no superlattice reflections in either diffraction pattern, confirming the absence of the ordered $L1_2$ precipitates. The time needed for particle dissolutions is called the incubation time hereforth.

Optical micrographs of directionally recrystallized high-purity Ni, Ni-3Al and Ni-12Al Figure 3-5 show optical micrographs of directionally recrystallized high-purity Ni at 1000°C, 1100°C and 1200°C at different drawing velocities. Analysis of the optical micrographs revealed several important qualitative trends:

(1) The grain aspect ratio of high-purity Ni is larger at the medium drawing velocity than for either the slow (2 mm/h at 1000°C and 1100°C, 2 mm/h and 5 mm/h at 1200°C) or the fast drawing velocities (above 50 mm/h at 1000°C, and above 100 mm/h at 1100°C and 1200°C).

(2) The number of equiaxed grains in high-purity Ni is smaller at the medium drawing velocity than for either the slow or the fast drawing velocities;

(3) The number of equiaxed grains in high-purity Ni is smaller at the lower annealing temperature than at higher annealing temperatures at slow drawing velocity;

Figure 6-8 show optical micrographs of directionally recrystallized Ni-3Al at 1000^{o}C, 1100^{o}C and 1200^{o}C at different drawing velocities. Comparing with the high-purity Ni counterparts, optical micrographs revealed several important qualitative trends:

(1) The upper limit of the drawing velocity that can form columnar grains is lower for Ni-3Al than for high-purity Ni.

(2) The average grain length and width of Ni-3Al is larger than those for high-purity Ni.

(3) The number of equiaxed grains is much lower in Ni-3Al than in Ni when the drawing velocity is low.

(4) Unlike the high-purity Ni counterpart, the average grain length and grain width of columnar grains didn't change much at different annealing temperatures.

Figure 9-11 show optical micrographs of directionally recrystallized Ni-12Al with small particles at 1100^{o}C, Ni-12Al with small particles at 1200^{o}C, and Ni-12Al with large particles at 1200^{o}C at different drawing velocities. Comparing with the Ni-3Al counterparts, optical micrographs revealed several important qualitative trends:

(1) The incubation length increases with increasing particle size, drawing velocity and decreasing annealing temperature.

(2) Ni-12Al with small particles can form columnar grains, but at a higher annealing temperature compared to its particle-free Ni-3Al counterpart, whilst columnar grains were not formed in Ni-12Al with large γ' particles for the same annealing parameters.

(3) Columnar grains only formed after the γ' particles dissolved. γ' particle dissolution is not a trigger for columnar grain formation but is simply a prerequisite.

(4) The grain length/width of Ni-12Al with small particles was much smaller than Ni-3Al while the number of equiaxed grains in Ni-12Al was much larger than Ni-3Al

Figure 12 (a) and (b) shows optical microscope images of cold-rolled high-purity Ni annealed at 1000°C and 1100°C at a variety of drawing velocities. Three phenomena were evident in the OM images from the three runs at each temperature:

(1) The upper drawing speed for columnar grains to propagate is higher than that for columnar grains to be nucleated, which is 30 mm/h at 1000°C and 100 mm/h at 1100°C, as shown in Figures 3 and 4.

(2) The columnar grain growth front broke down when the drawing velocity was increased.

(3) The growth front breakdown happened in two ways: (1) some grains kept growing while others stopped, and (2) part of a grain kept growing while another part was impeded.

EBSD study of directional recrystallized high-purity Ni, Ni-3Al and Ni-12Al

Figures 13 and 14 shows EBSD maps of directionally recrystallized high-purity Ni at 1000°C at various drawing velocities, and Ni-3Al at 1200°C at various drawing velocities. It is shown that:

(1) The small equiaxed grains ahead of columnar grains have a sharp cube texture with minor non-cube textures. Boundaries between cube-textured grains were low-angle boundaries (texture pinning) and boundaries between cube-textured grains and non-cube textured grains are high angle boundaries.

(2) The cube texture is sharper and less non-cube textured grains were found in Ni-3Al than high-purity Ni even through Ni-3Al samples were DRed at higher temperature.

(3) The cube texture is sharper and less non-cube-textured grains were found when the drawing velocity was slower.

(4) Three kinds of boundaries: boundaries between columnar grains (CC boundaries), boundaries between columnar grains and small grains ahead of them and island grain boundaries were found in DRed materials.

Figure 15 shows EBSD maps of Ni-12Al with small particles directionally recrystallized at 1200^{o}C at various drawing velocities. Comparing to Ni-3Al, several phenomena were observed,

(1) The cube texture was less sharp and more non-cube textured grains were found in Ni-12Al with small particles.

(2) Small grains ahead of columnar grains still have a sharp cube-texture and texture pinning still exist.

Figure 16 shows an EBSD map of a Ni-12Al with large particles directionally recrystallized at 1200^{o}C at 10 mm/h. It is shown that:

(1) The dominant texture of small equiaxed grains was no longer cube-textured grains before obvious grain growth happened. Texture pinning was absent in Ni-12Al samples with large particles.

Figure 17 shows a typical EBSD mapping where one columnar grain stopped growth while the other kept on going in a high-purity Ni sample annealed at 1000°C. Figure 17 (b) shows the [001] pole figure of columnar grains 1, 2, 3 and 4 in Figure 17 (a) with the color coded according to the EBSD mapping. It is shown that columnar grains 1 and 4 had a {124}<211> orientation, which has a 40°/<111> rotation relationship with cube texture and has the highest grain boundary mobility, while columnar grains 2 and 3 are non-{124}<211> grains. Further, columnar grain 2 is further away from the {124}<211> orientation than columnar grain 3. It is also evident that the growth of columnar grain 1 was not hindered and columnar grain 2 stopped growing while columnar grain 3 was retarded but kept growing sideways.

Figure 18 shows a typical EBSD map taken from where part of a grain kept growing while another part was impeded in a sample annealed at 1100°C. The low-angle boundaries or CSL boundaries are marked on the map. It is evident that the part of boundary that stopped growing were pinned by low-angle boundaries or low CSL boundaries, which have relatively low mobility. When the drawing velocity was increased, they cannot follow the hot zone as easily as other boundaries and were left behind, which caused the second type of growth front breakdown.

Statistics based on EBSD results

Figure 19 (a), (b) and (c) show [001] pole figures of all columnar grains in Ni-12Al with small particles, Ni-3Al and high-purity Ni. It is evident that the major texture for columnar grains in high-purity Ni is the {124}<211> texture, which mean columnar grains in high-

purity Ni have a 40º/<111> rotation relationship with the cube texture, while Ni-3Al has a near random texture, which means CE boundaries in Ni-3Al are random high-angle boundaries. The texture in Ni-12Al is less random than in Ni-3Al while the {124}<211> content is obviously stronger.

Figure 20 shows the character of the CC boundaries for both Ni-3Al and Ni-12Al. The majority of CC boundaries in Ni-3Al are twin boundaries while the majority CC boundaries in Ni-12Al are high-angle boundaries.

Figure 21 shows the character of the island boundaries for high-purity Ni, Ni-3Al and Ni-12Al. The percent of twin boundaries is higher in Ni-3Al than high-purity Ni and Ni-12Al. There is an obvious increase of high-angle island boundaries in Ni-12Al.

Scientific Significance and Army Value

The focus of this project was to obtain fundamental understanding of how solute and particles interact with processing parameters to affect directional recrystallization. This research first showed proof that solute drag was not only misorientation-angle dependent but also misorientation-axis dependent , which can be used as theoretical guidance to control texture and boundaries in bulk material, through which specific material properties can be obtained. This study also proved that particle dissolution was a prerequisite for columnar grain formation and the key factor that controls columnar grain formation was texture pinning, which can be used as guide for Ni-based superalloy design for turbine blades purpose. Furthermore, this conclusion can be used for directional recrystallization of other military materials like tungsten. The prediction that the “Drawing velocity limited needed for

columnar grains propagation is higher than columnar grain formation" was also confirmed experimentally, which can increase the efficiency of directional recrystallization by initiating the process at lower drawing velocity and increase the drawing velocity later.

Publications

[1] C. Yang and I. Baker, "Elevated temperature directional recrystallization of high- purity nickel", Philosophical Magazine, **99(9)** (2019) 1057-1078. doi.org/10.1080/14786435.2019.1576936

[2] C. Yang and I. Baker, "Breakdown of growth front at elevated drawing velocity during directional recrystallization", Philosophical Magazine Letters, **99(5)** (2019) 167-172. doi.org/10.1080/09500839.2019.1644459

[3] C. Yang and I. Baker, "Effect of solute on microstructural evolution during directional recrystallization", Journal of Alloys and Compounds, **815** (2020). 152358

doi.org/10.1016/j.jallcom.2019.152358

[4] C. Yang and I. Baker, "Effect of soluble particles on microstructural evolution during directional recrystallization", Acta Materialia, *in press*.

[5] C. Yang and I. Baker, "Directional Recrystallization: A review". submitted to International Materials Reviews (INVITED)

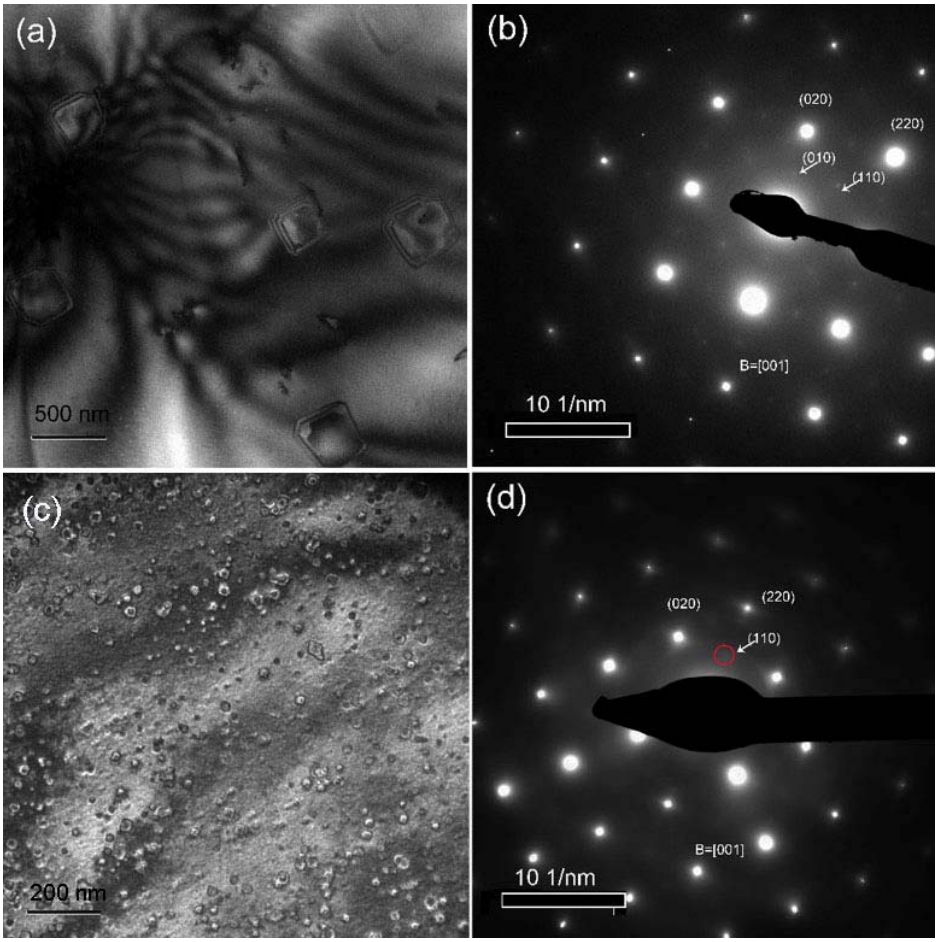

Figure 1: (a) Bright field image of Ni-12Al alloy annealed for 48 h at 700^{o}C after homogenization at 1000^{o}C for 1 h ,(b) diffraction pattern of (a) at [001] zone axis, (c) dark field image of the Ni-12Al alloy annealed at 700^{o}C for 30 minutes after homogenization at 1000^{o}C for 1 h, and (d) diffraction pattern of (c) at the [001] zone axis.

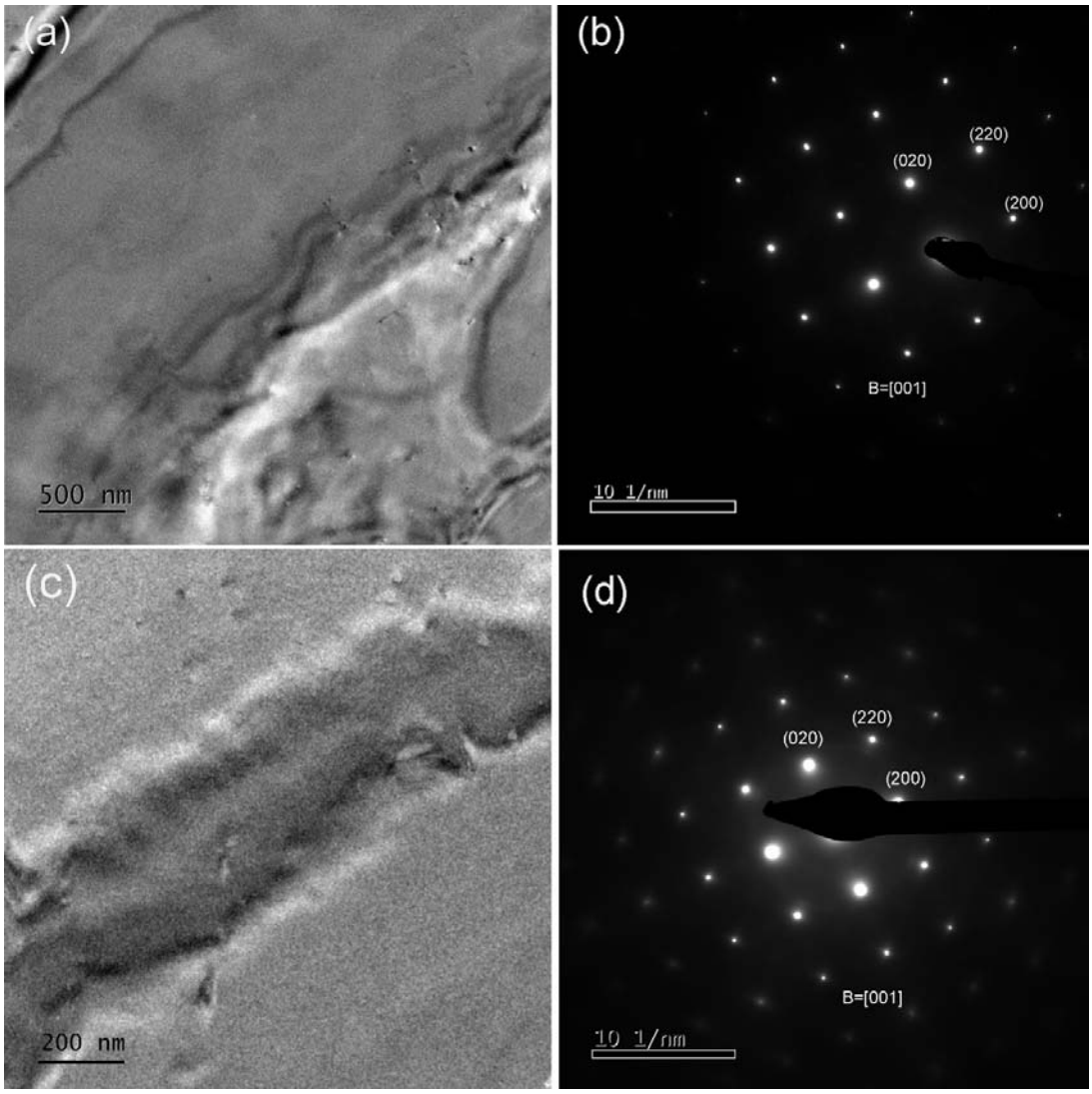

Figure 2: (a) Bright field image of a small-particle sample DRed at 1200°C, 10 mm/h taken from columnar grain region (b) corresponding diffraction pattern of (a) under zone axis [001], (c) bright field image of a large-particle sample DRed at 1200°C, 10 mm/h taken from region where obvious grain growth happened and (d) corresponding diffraction pattern of (c) at the zone axis [001].

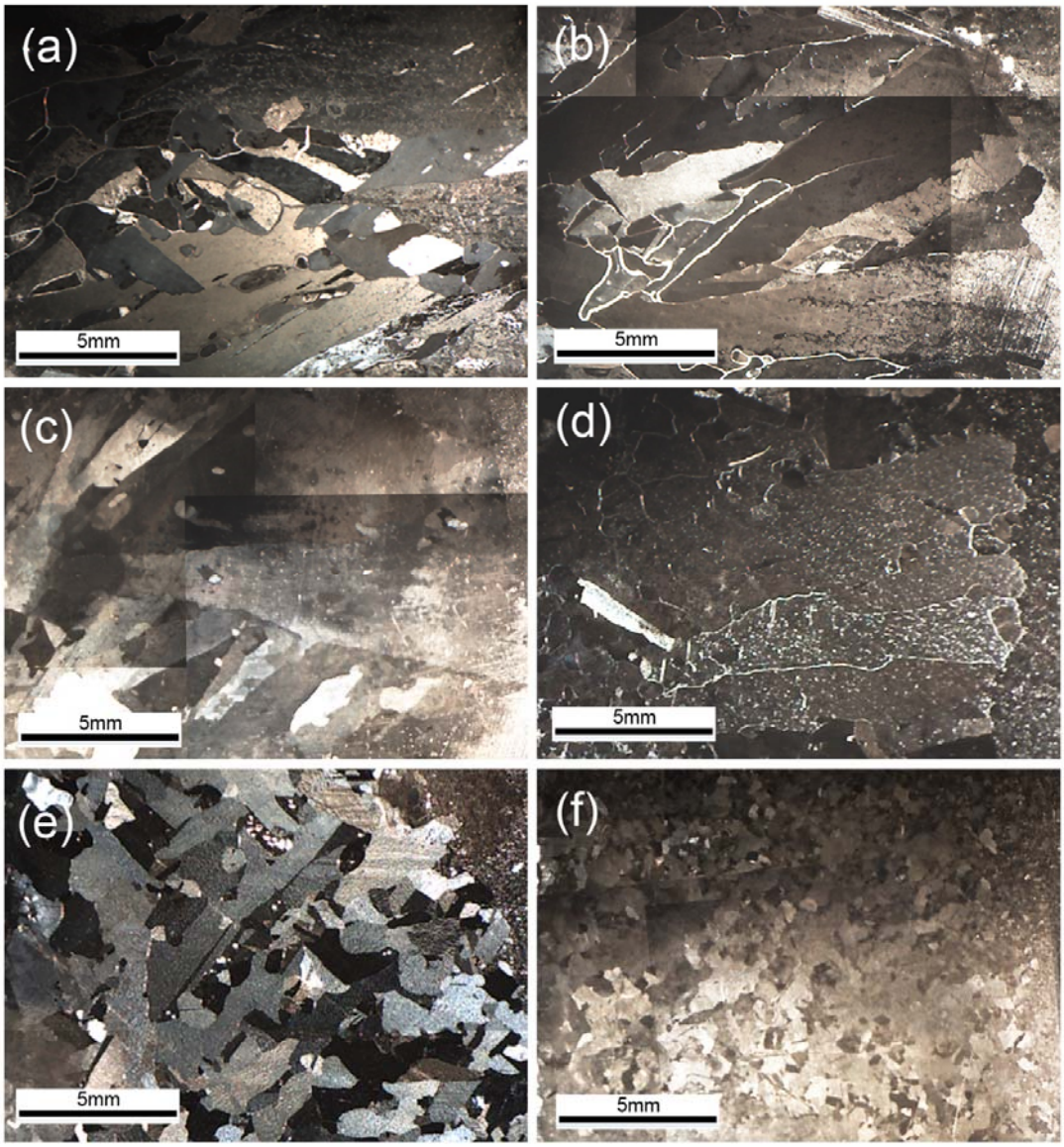

Figure 3: Optical micrographs of cold-rolled high-purity Ni annealed at 1000 ^{o}C at drawing velocities of (a) 2 mm/h, (b) 5 mm/h, (c) 10 mm/h, (d) 30 mm/h, (e) 50 mm/h, and (f) 100 mm/h. The hot zone movement is from left to right.

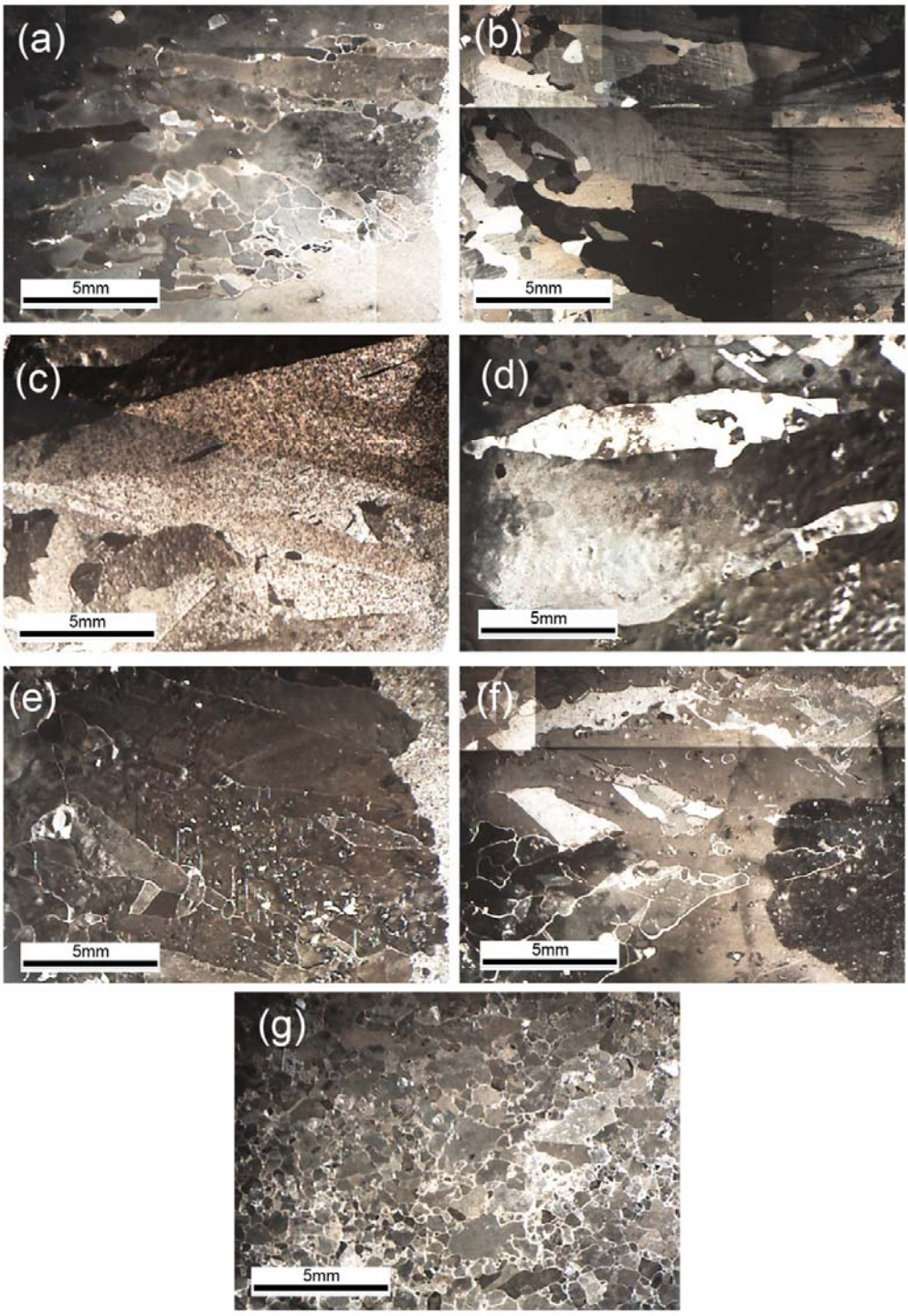

Figure 4: Optical micrographs of cold-rolled high-purity Ni annealed at 1100 ^{o}C at drawing velocities of (a) 2 mm/h, (b) 5 mm/h, (c) 10 mm/h, (d) 30 mm/h, (e) 50 mm/h, (f) 100 mm/h, and (g) 200 mm/h. The hot zone movement is from left to right.

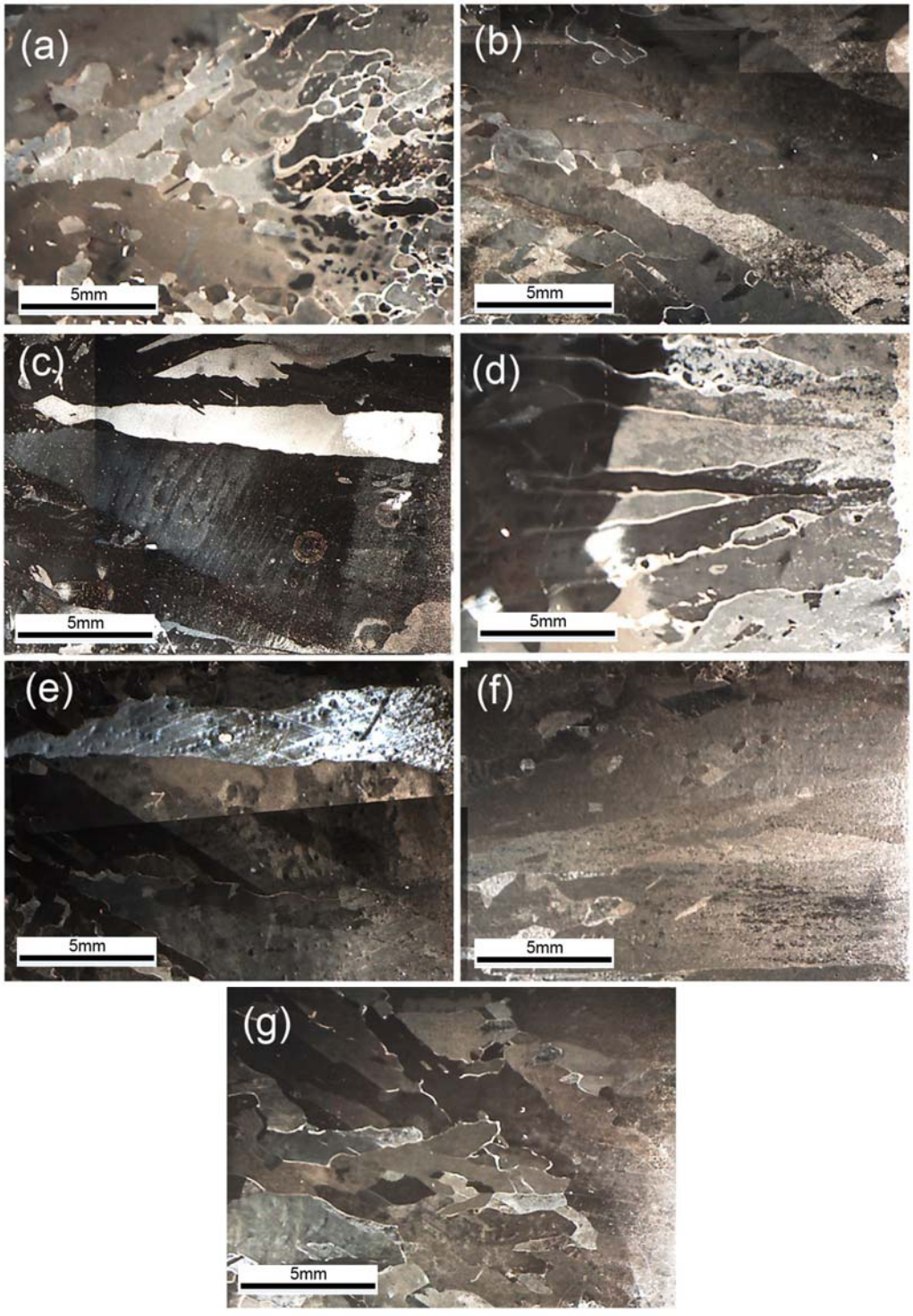

Figure 5: Optical micrographs of cold-rolled high-purity Ni annealed at 1200 °C at drawing velocities of (a) 2 mm/h, (b)5 mm/h, (c) 10 mm/h, (d) 30 mm/h, (e) 50 mm/h, (f) 100 mm/h, and (g) 200 mm/h. The hot zone movement is from left to right.

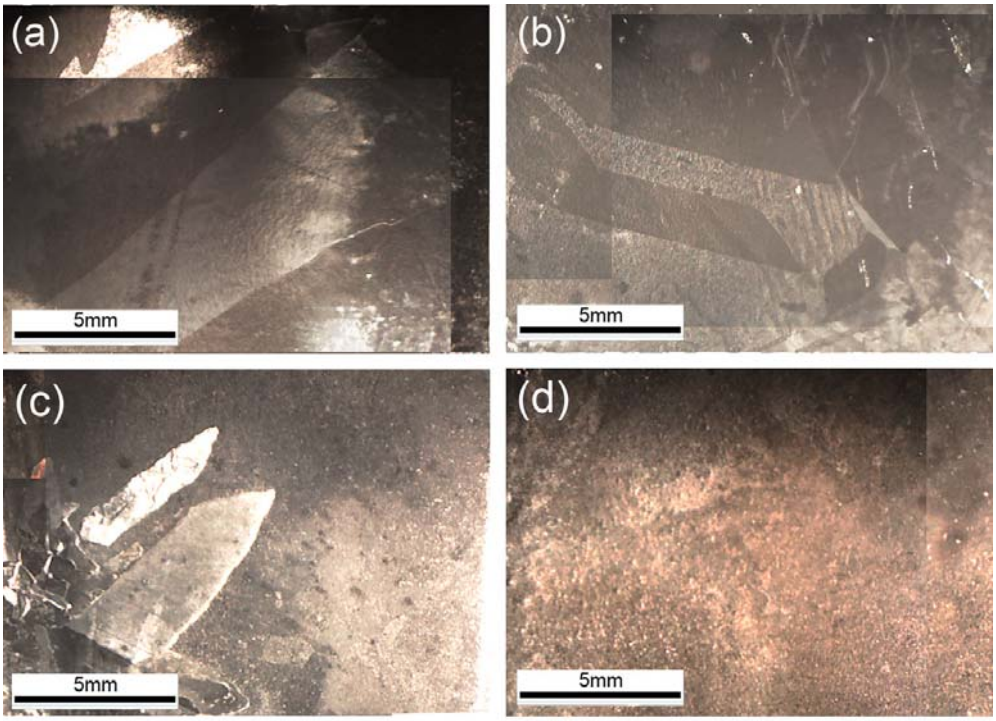

Figure 6: Optical micrographs of cold-rolled Ni-3Al annealed at 1000 °C at drawing velocities of: (a) 2mm/h, (b) 5 mm/h, (c) 10 mm/h, (d) 30 mm/h. The hot zone movement is from left to right.

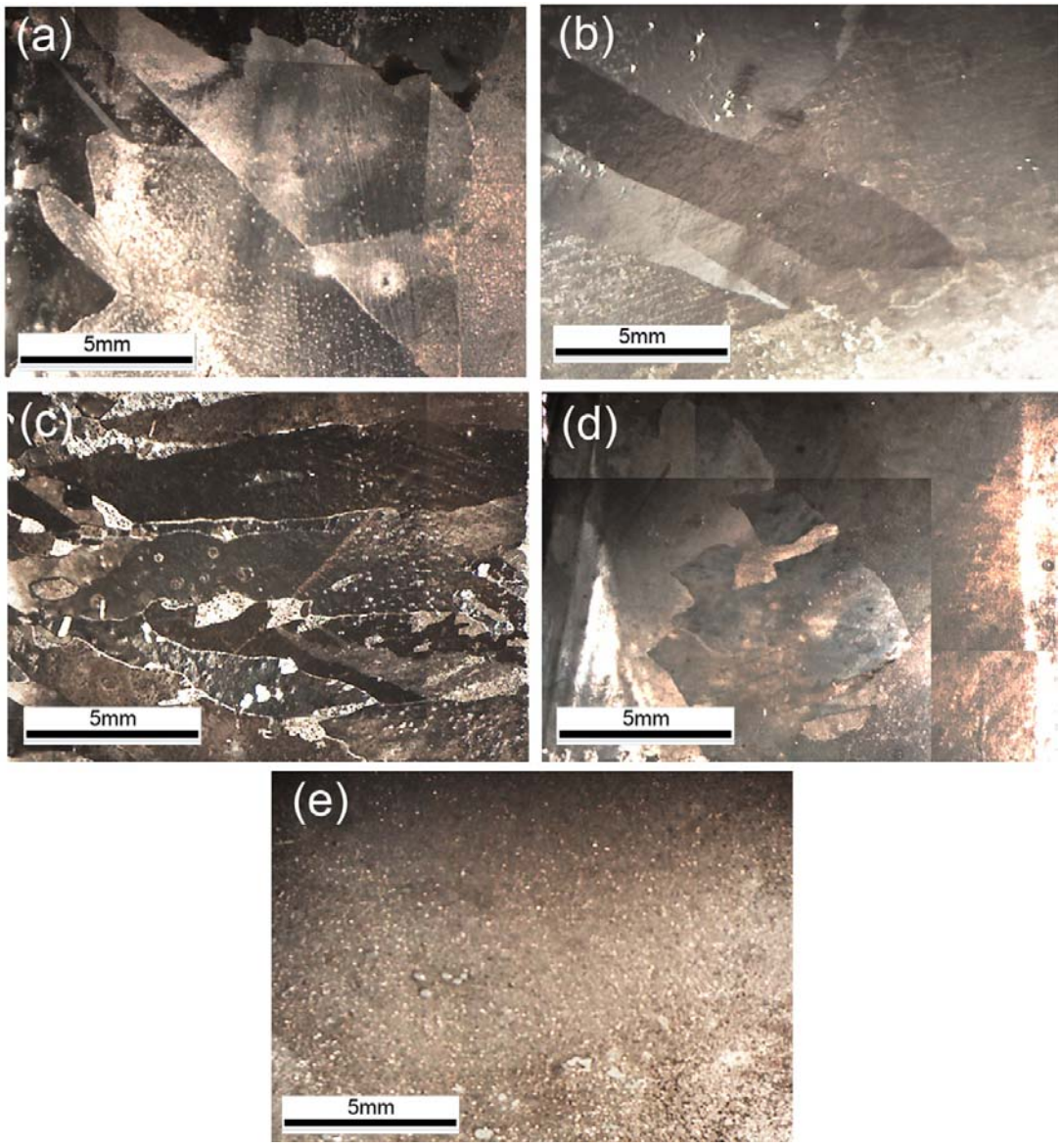

Figure 7: Optical micrographs of cold-rolled Ni-3Al annealed at 1100 °C at drawing velocities of:(a) 2mm/h, (b) 5 mm/h, (c) 10 mm/h, (d) 30 mm/h and (e) 50 mm/h. The hot zone movement is from left to right.

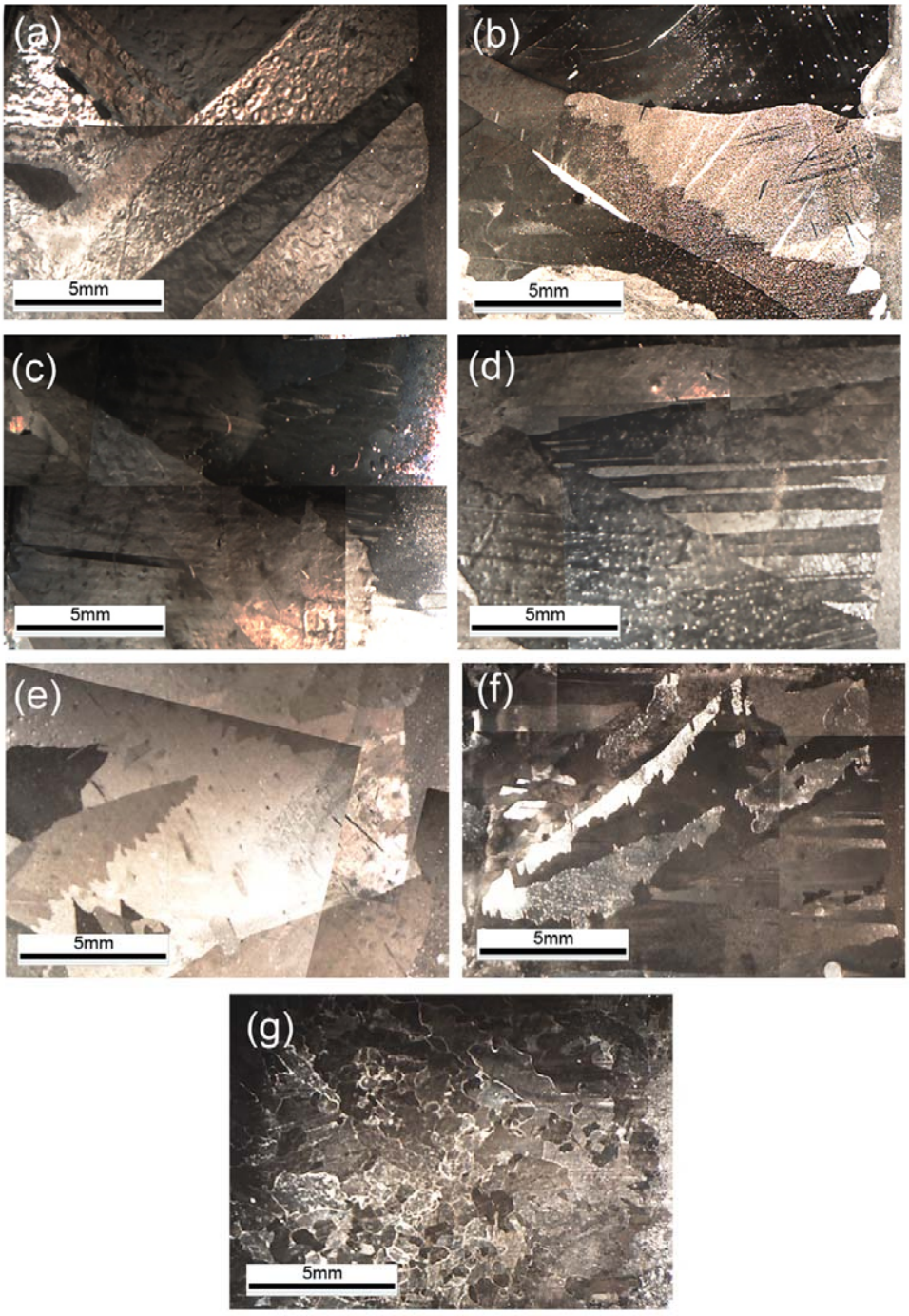

Figure 8: Optical micrographs of cold-rolled Ni-3Al annealed at 1200 °C at drawing velocities of (a) 2mm/h, (b)5 mm/h, (c) 10 mm/h, (d) 30 mm/h, (e) 50 mm/h, (f) 100 mm/h, and (g) 200 mm/h. The hot zone movement is from left to right.

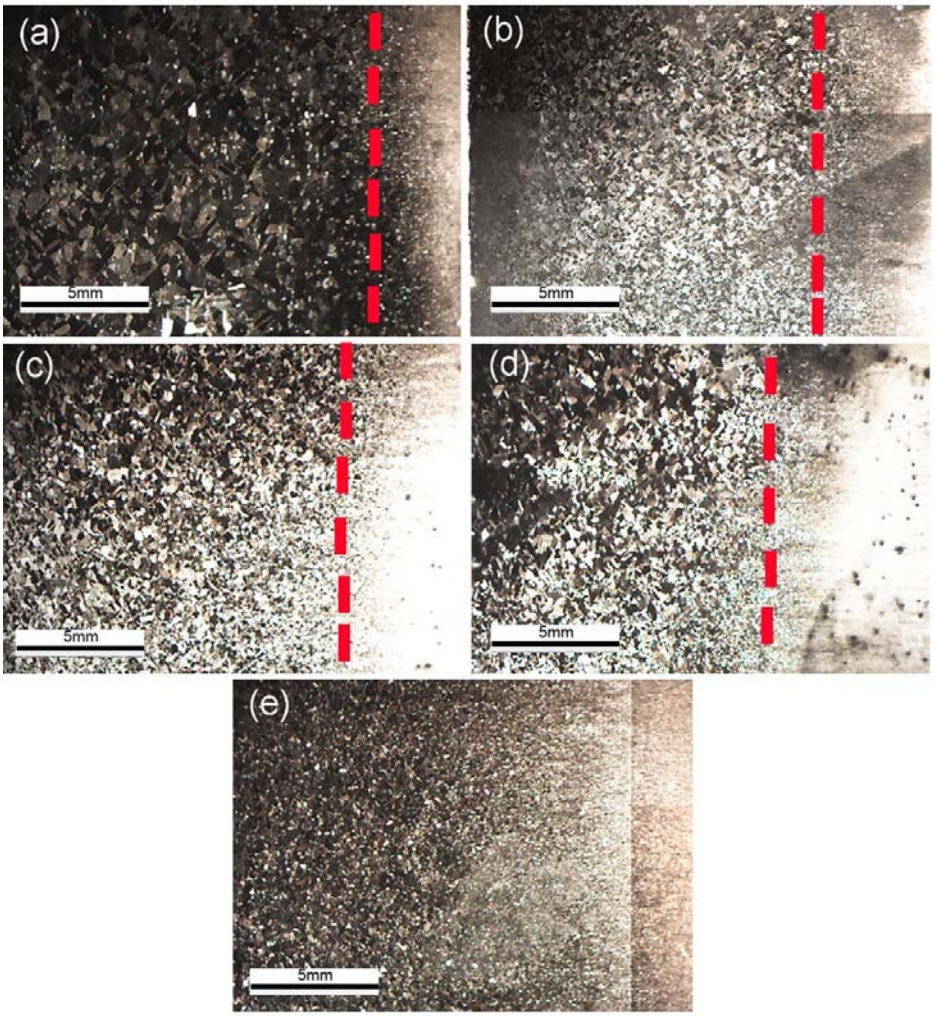

Figure 9: Optical micrographs of cold-rolled Ni-12Al with small particles DRed at 1100 °C at drawing velocities of (a) 2 mm/h, (b)5 mm/h, (c) 10 mm/h, (d) 30 mm/h and (e) 50 mm/h. The hot zone movement is from left to right. The boundaries where the grain size changed are marked with red dashed lines.

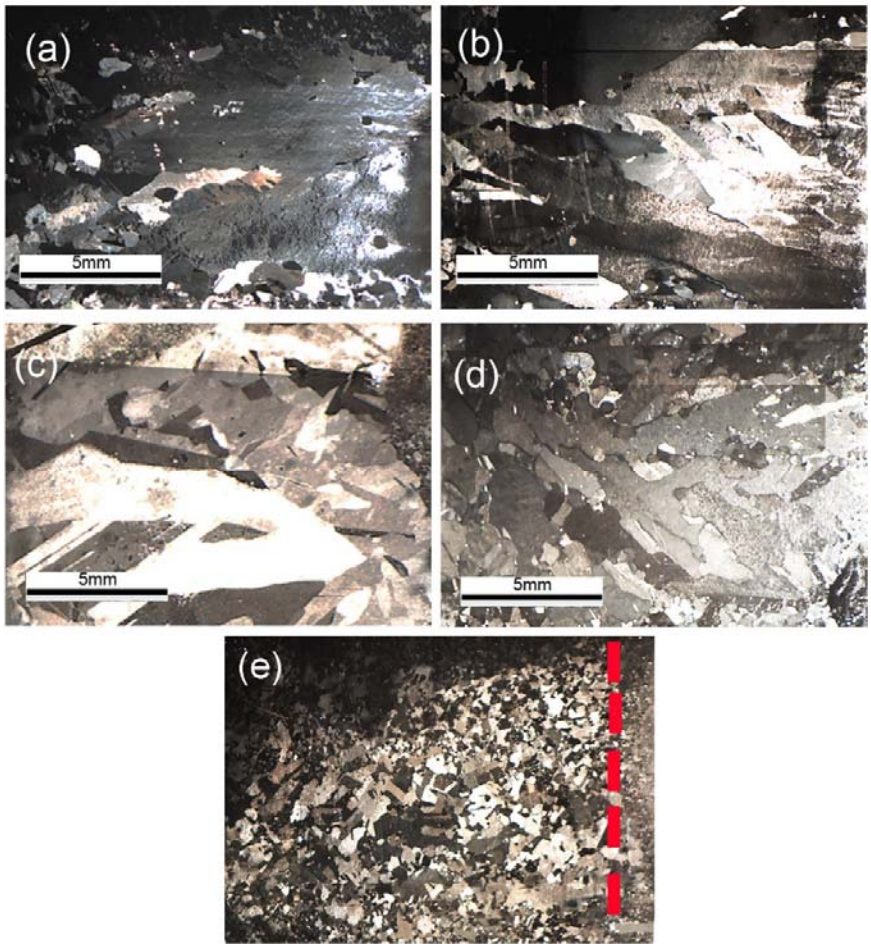

Figure 10: Optical micrographs of cold-rolled Ni-12Al with small particles DRed at 1200 °C at drawing velocities of (a) 2 mm/h, (b)5 mm/h, (c) 10 mm/h, (d) 30 mm/h and (e) 50 mm/h. The hot zone movement is from left to right. The boundaries where the grain size changed are marked with red dashed lines.

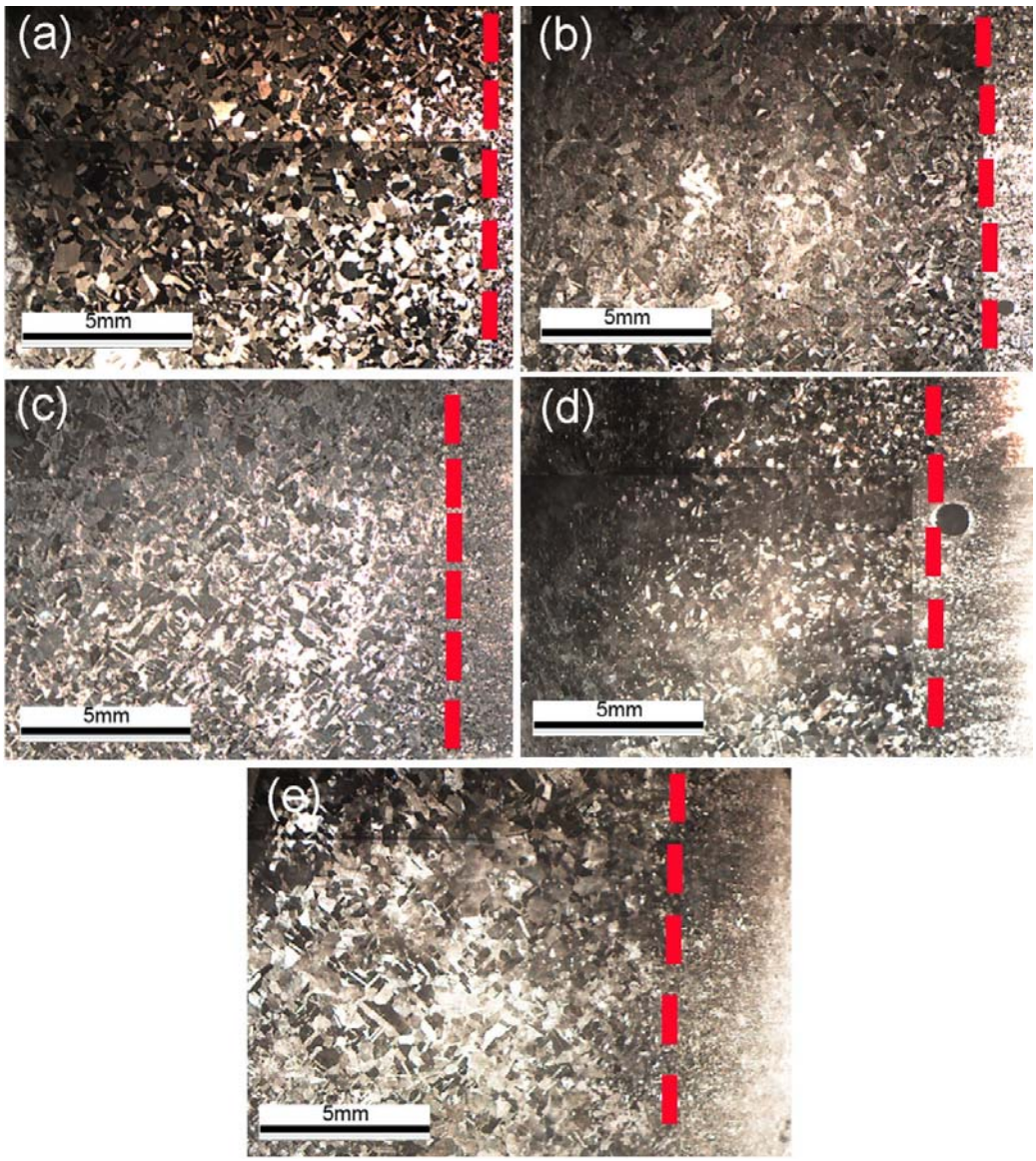

Figure 11: Optical micrographs of cold-rolled Ni-12Al with large particles DRed at 1200 °C at drawing velocities of (a) 2 mm/h, (b)5 mm/h, (c) 10 mm/h, (d) 30 mm/h and (e) 50 mm/h. The hot zone movement is from left to right. The boundaries where the grain size changed are marked with red dashed lines.

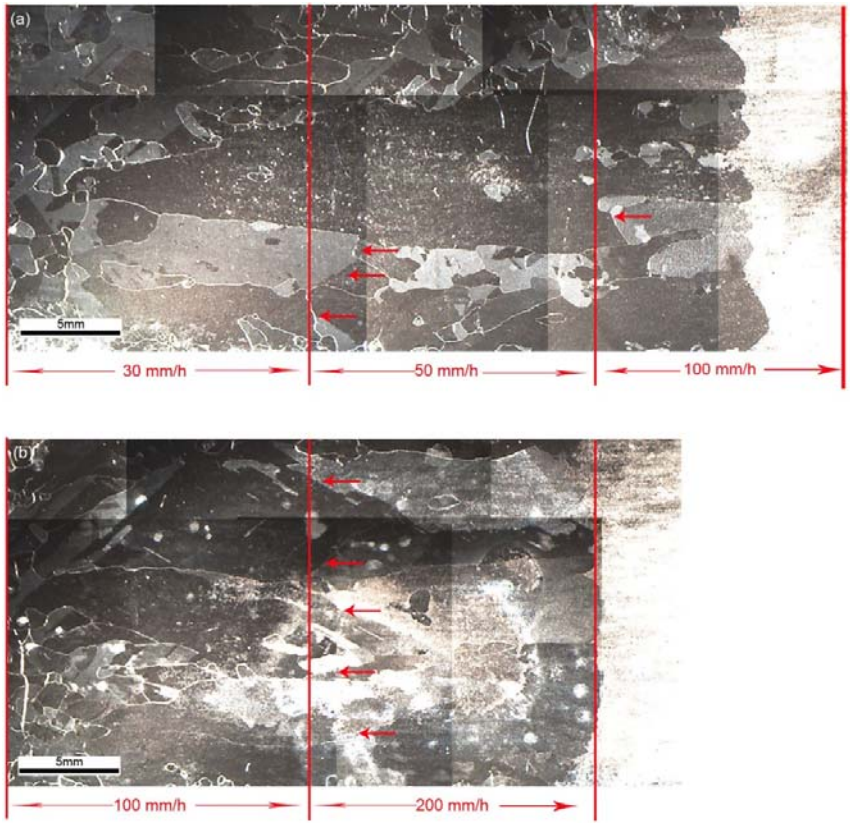

Figure 12: Optical microscope images of cold-rolled high-purity Ni directionally annealed at (a)1000°C and (b) 1100°C. Growth direction is from left to right. The drawing velocity was increased during processing as shown. Where grains stopped growing when the drawing velocity was increased is marked by red arrows.

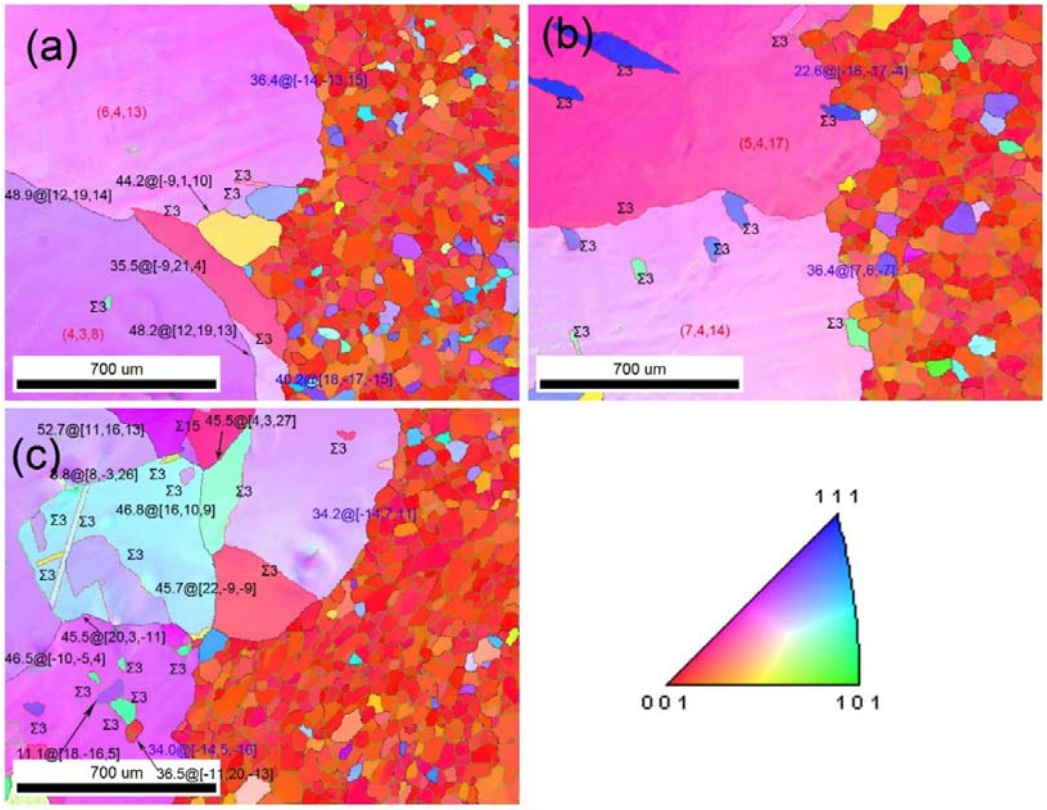

Figure 13: EBSD mapping of high-purity Ni sample annealed at 1000°C at (a) 2 mm/h, (b) 10 mm/h, (c) 50 mm/h. Maps were taken from where columnar grains end.

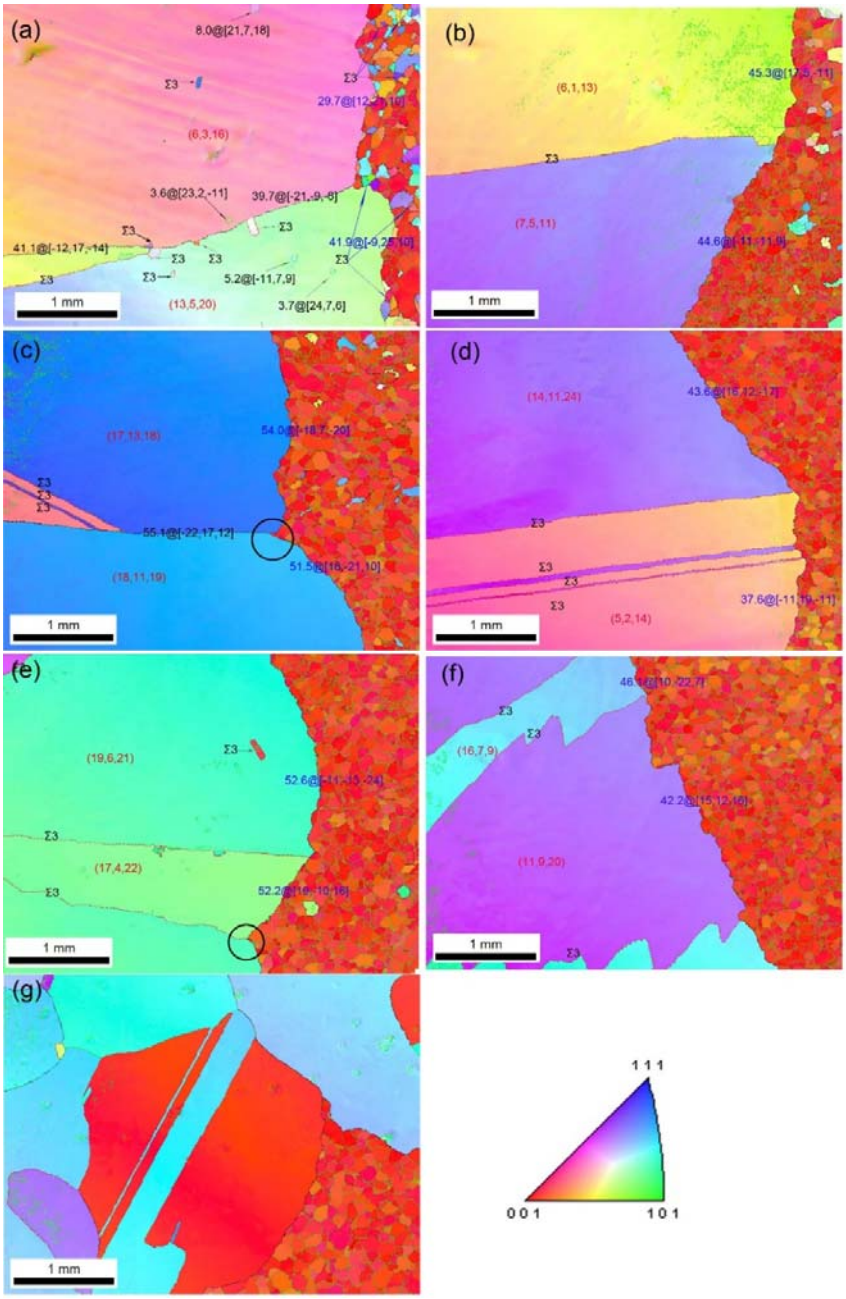

Figure 14: EBSD mapping of Ni-3Al sample annealed at 1200 ^{o}C at (a) 2 mm/h, (b) 5 mm/h, (c) 10 mm/h, (d) 30 mm/h, (e) 50 mm/h, (f) 100 mm/h and (g) 200 mm/h. Island grain boundaries were indicated by black arrows, twin boundaries between small non-cube grains were indicated by blue arrows and CE boundaries that pinned by CC boundaries were indicated by black circle.

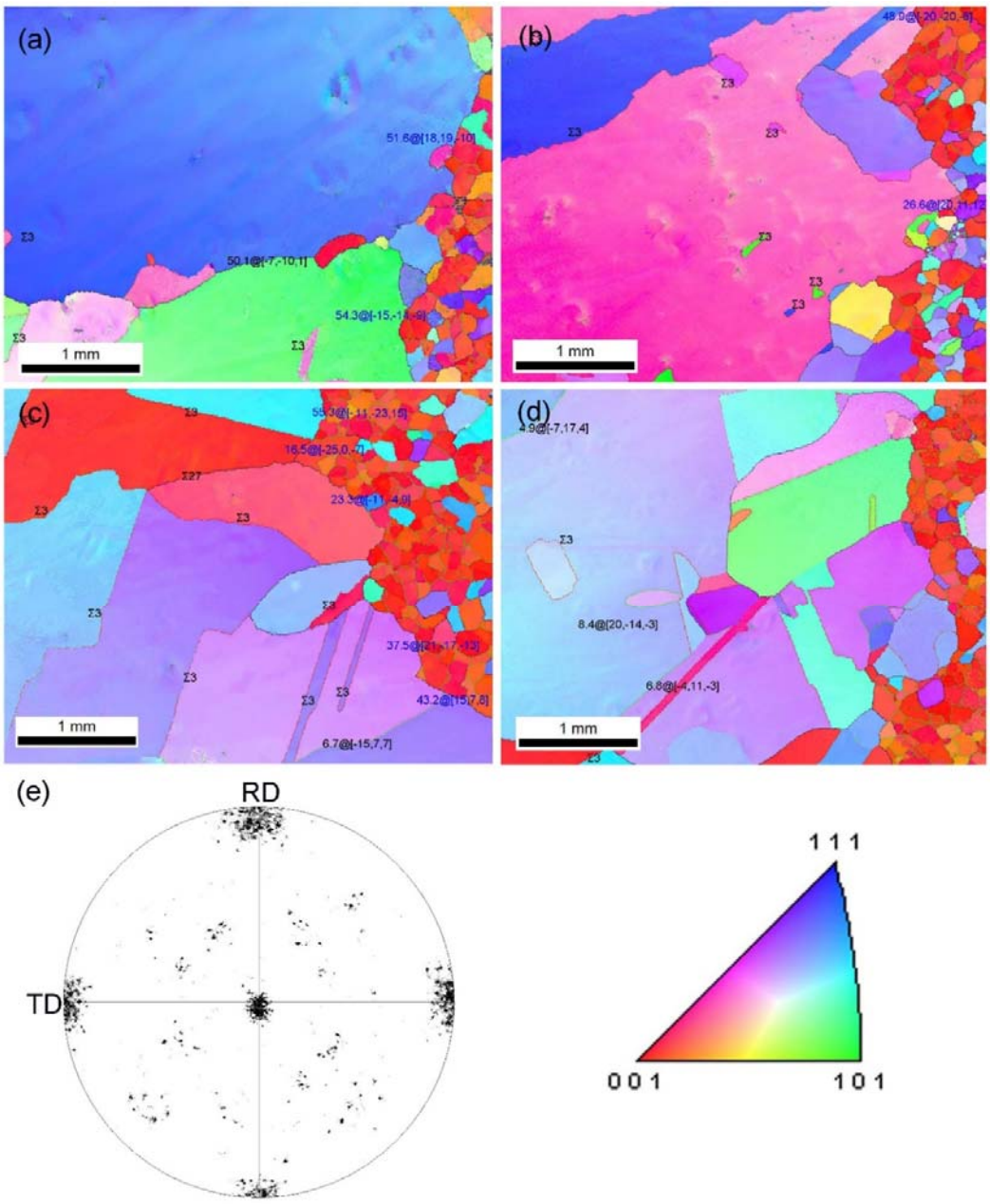

Figure15: EBSD mapping of small-particle sample DRed at 1200 °C at (a) 2 mm/h, (b) 5 mm/h, (c) 10 mm/h and (d) 30 mm/h. (e) is [001] pole figure of small grains ahead of columnar grains in (c).

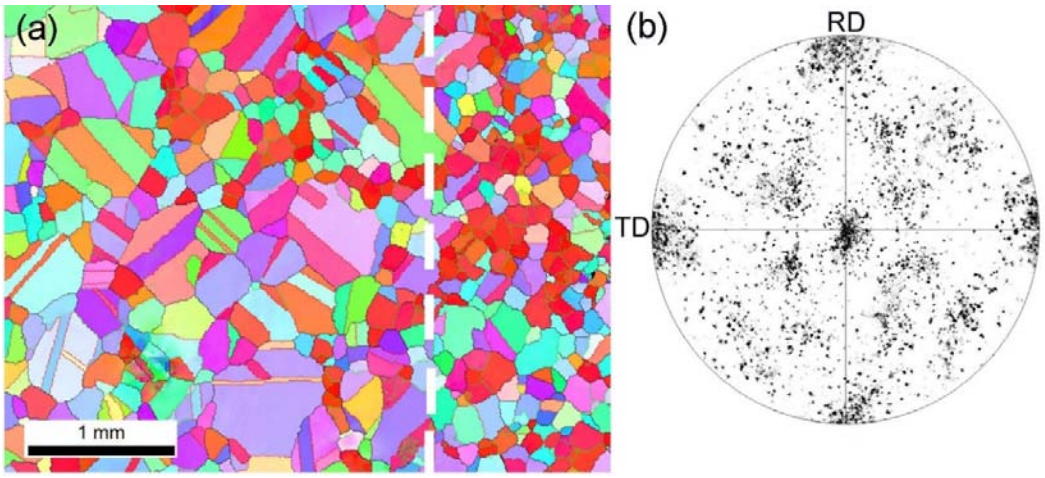

Figure 16: (a) EBSD mapping of a large-particle sample DRed at 1200 ^{o}C at 10 mm/h and (b) corresponding [001] pole figure of small grains on the right of the white line in (a), which indicates the boundaries where obvious grain growth happened.

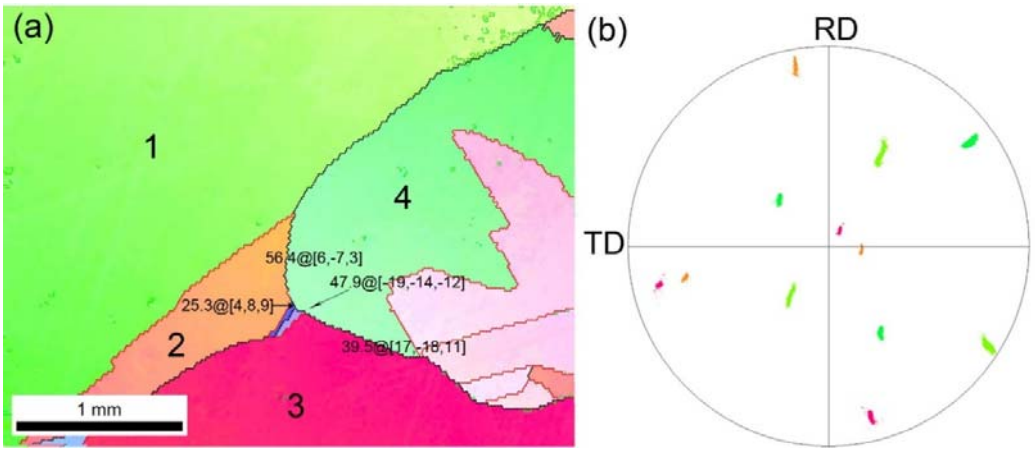

Figure 17: (a) Typical EBSD map from where growth front breaks down by some columnar grains stopped growing in a high-purity Ni sample annealed at 1000°C. (b) corresponding [001] pole figure of columnar grains 1,2,3 and 4 in (a). The hot zone movement is from left to right.

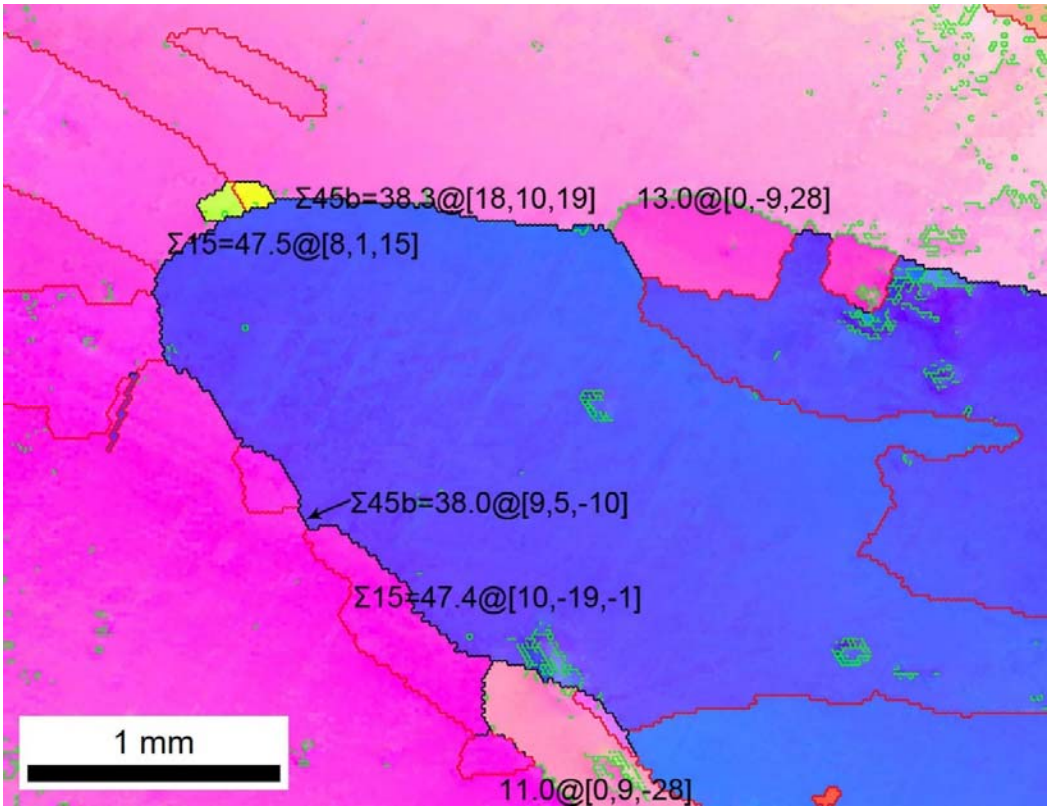

Figure 18: Typical EBSD map of where growth front breaks by some part of a columnar grains got impeded in a high-purity Ni sample annealed at 1100°C. The hot zone movement is from left to right.

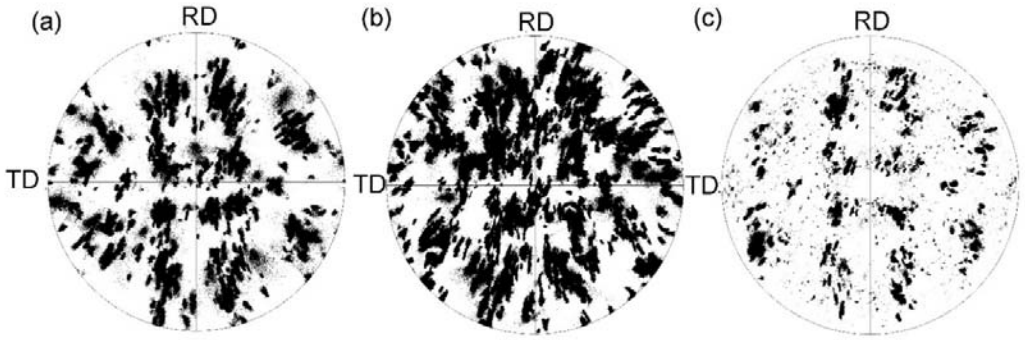

Figure 19: [001] pole figure of all the columnar grains in DRed (a) small particles Ni-12Al (2) Ni-3Al and (c)high-purity Ni.

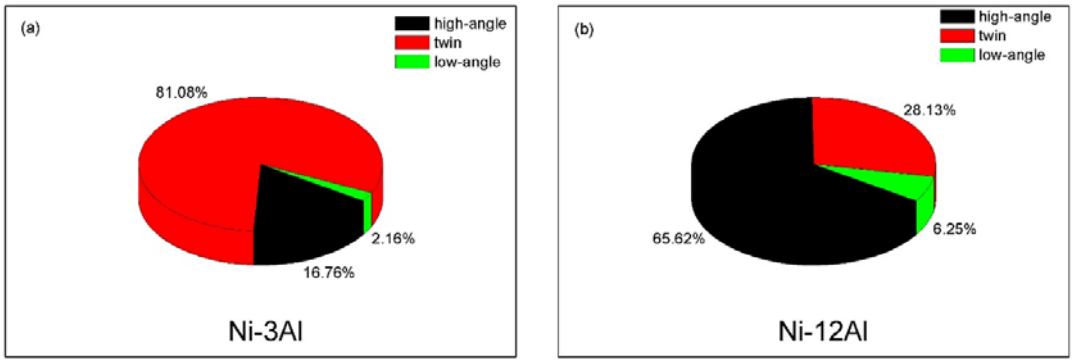

Figure 20: Character of all CC boundaries in DRed (a) Ni-3Al and (b)small-particle Ni-12Al samples

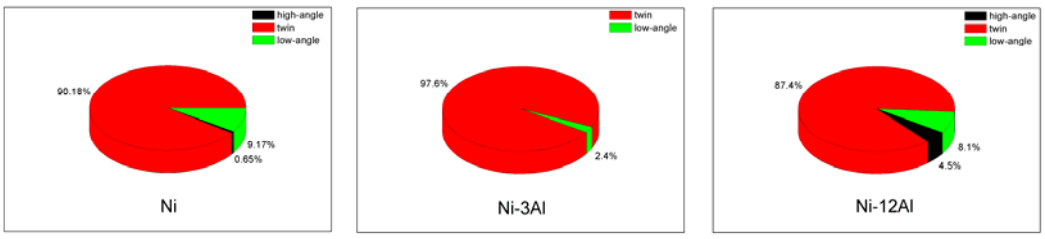

Figure 21: Character of all island grain boundaries in DRed high-purity Ni, Ni-3Al and small-particle Ni-12Al samples.